ACS central science

Research Article

http://pubs.acs.org/journal/acscii

Electrochemically Expandable Soft Carbon as Anodes for Na-Ion Batteries

Wei Luo,[†] Zelang Jian,[†] Zhenyu Xing, Wei Wang, Clement Bommier, Michael M. Lerner, and Xiulei Ji*

Department of Chemistry, Oregon State University, Corvallis, Oregon 97331-4003, United States

Supporting Information

ABSTRACT: Na-ion batteries (NIBs) have attracted great attention for scalable electrical energy storage considering the abundance and wide availability of Na resources. However, it remains elusive whether carbon anodes can achieve the similar scale of successes in Na-ion batteries as in Li-ion batteries. Currently, much attention is focused on hard carbon while soft carbon is generally considered a poor choice. In this study, we discover that soft carbon can be a high-rate anode in NIBs if the preparation conditions are carefully chosen. Furthermore, we discover that the turbostratic lattice of soft carbon is electrochemically expandable, where *d*-spacing rises from 3.6 to 4.2 Å. Such a scale of lattice expansion only due to the Na-ion insertion was not known for carbon materials. It is further learned that portions of such lattice expansion are highly reversible, resulting in excellent cycling performance. Moreover, soft carbon delivers a good capacity at potentials above 0.2 V, which enables an intrinsically dendrite-free anode for NIBs.

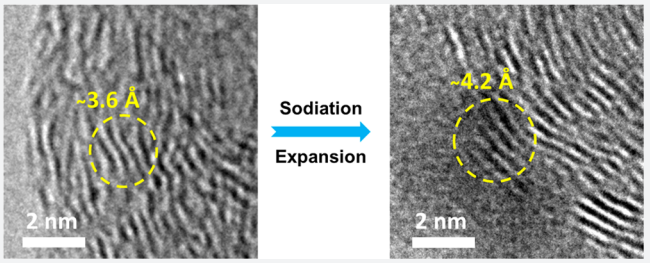

INTRODUCTION

Electrical energy storage (EES) technologies are instrumental to not only store clean energy from renewable energy sources and reduce the dependence on depleting fossil fuels but also significantly decrease the emission of greenhouse gases.[1−3] Among different EES technologies, Li-ion batteries (LIBs) have remained the choice for portable electronic devices and some electric vehicles (EVs) due to the high energy/power density and long cycle life.[4−8] However, concerns of large-scale deployment of LIBs arise due to the rarity and geographically uneven distribution of Li resources, which triggers increasing attention to an important alternative of LIBs: Na-ion batteries (NIBs).[9−16] Based on similar alkali metal chemistries as in LIBs, NIBs show the promise to emerge as a grid-level EES solution. This has to do with the sustainability advantage originated from the low cost, abundance, and wide availability of Na resources.[17−19] The challenges associated with NIBs typically come from the facts that Na ions are much larger than Li ions and Na has unique lattice energy and desolvation energy, which forbids the extension of rich knowledge of LIBs to NIBs. This is particularly true for the anode.[20−26] Graphite, the most practical choice for LIBs, exhibits an extremely low capacity for NIBs, corresponding to NaC_{64}.[27,28]

Among various anode candidates, hard carbon anodes have attracted most attention for NIBs due to high capacity and relatively high first-cycle coulombic efficiency (1st cycle CE).[29−33] However, about 60% of the capacity from hard carbon is contributed by sodiation below 0.2 V vs Na^+/Na (Figure S1).[34] This low potential plateau makes hard carbon energetically favorable as an anode but causes a safety concern of Na dendrite formation when high current densities are used. Furthermore, the tortuous atomic structure of hard carbon suffers low electronic and ionic conductivity, which leads to a relatively poor rate capability. In contrast to the non-graphitizable hard carbon, soft carbon represents the graphitizable nongraphitic carbon with a higher electronic conductivity, whose graphitization degrees and interlayer distance can be tuned by a thermal treatment.[35] The pioneering study by Doeff et al. demonstrated that reversible sodiation of a petroleum coke soft carbon results in the formation of NaC_{24} by delivering a capacity of ∼90 mAh/g.[36] The subsequent studies investigated other soft carbons, such as pitch-derived soft carbon,[31] carbon black,[37] and mesitylene-derived spherical carbon.[38] Most recently, it was reported that heteroatom-doped partially carbonized aromatic hydrocarbons exhibit high capacity values, i.e., above 300 mAh/g, for storing Na ions.[39,40] Nevertheless, despite the intriguing performance of these doped materials, the full performance potential of soft carbons has not been explored and well understood. It is also a practically relevant issue that more than 50% of the desodiation capacities of these doped materials are contributed from potentials higher than 1.0 V vs Na^+/Na, which limits the energy density if such materials are used in full cells. Therefore, caution is needed when comparing different carbon-based materials, where one should not compare capacity values without considering the operating potentials.

It is important to obtain fundamental understanding for the soft carbon anodes in NIBs, where a relatively pure carbon is focused. Herein, we report on the empirical correlation

Received: October 2, 2015
Published: November 23, 2015

DOI: 10.1021/acscentsci.5b00329
ACS Cent. Sci. 2015, 1, 516−522

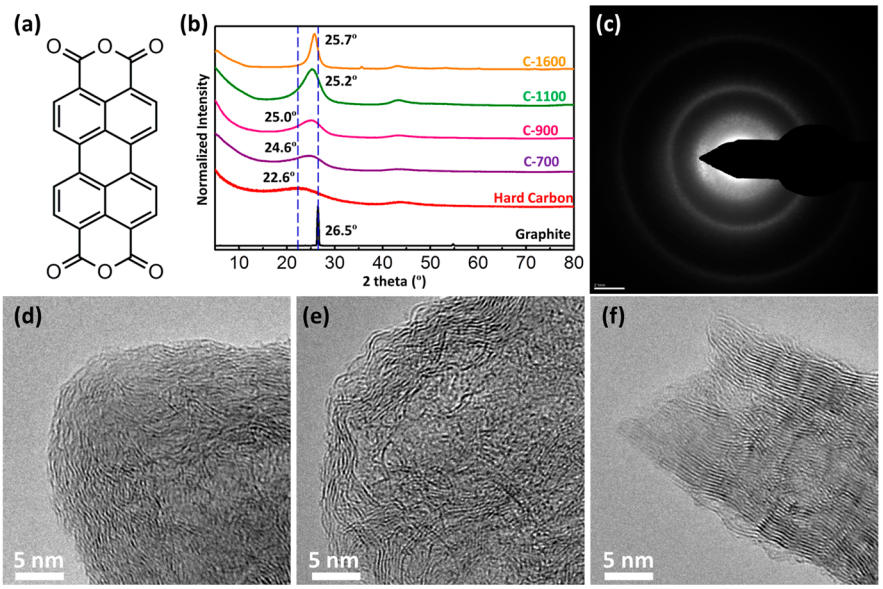

Figure 1. (a) Molecular structure of PTCDA. (b) XRD patterns of graphite, sucrose-derived hard carbon, and PTCDA-derived soft carbons. (c) SAED pattern of C-900. (d–f) HRTEM images of (d) C-900, (e) C-1100, and (f) C-1600.

Table 1. Pyrolysis Temperature, Interlayer Distance, Empirical *R* Value, Domain Thickness, 1st Cycle CE, Hydrogen Content, and BET Surface Area of PTCDA-Derived Soft Carbons and Sucrose-Derived Hard Carbon

sample no.	pyrolysis temp (°C)	interlayer distance (Å)	empirical *R* value	domain thickness (number of layers)	1st cycle CE (%)	content of hydrogen (wt %)	BET surface area (m^2/g)
C-700	700	3.62	1.94	3.8	62.6	0.93	13.6
C-900	900	3.56	2.67	4.8	67.6	0.12	20.2
C-1100	1100	3.53	4.47	6.2	60.5	0.12	32.8
C-1600	1600	3.46	10.94	13.8	47.5	<0.1	26.5
hard carbon[34]	1100	3.93	1.35	2.9	73.6		137.2

between the interlayer distance of pure soft carbon and its corresponding Na-ion storage properties, i.e., specific capacity as the figure of merit. A model soft carbon is synthesized by pyrolysis of 3,4,9,10-perylene-tetracarboxylic acid-dianhydride (PTCDA, $C_{24}H_8O_6$), which comprises a perylene aromatic core and two anhydride groups, as shown in Figure 1a. Our group has recently investigated PTCDA as a Na-ion storage electrode, which exhibits a high reversibility.[41] The ordered stacking of planar aromatic molecules of PTCDA in the β-form crystalline structure with the monoclinic $P2_1/c$ space group (Figure S2) facilitates PTCDA as an ideal precursor to prepare graphitizable soft carbon.[42−44] By using different pyrolysis temperatures, we are able to finely tune the interlayer distance between graphene sheets in the resulting soft carbons. When evaluated as NIB anodes, soft carbons with different interlayer distance exhibit vastly different performance. We, for the first time, identify that Na ions do intercalate in between the turbostratic graphene layers in the PTCDA-derived soft carbons with high capacities in the first sodiation, evidenced by a dramatic gallery expansion from ∼3.6 Å to ∼4.2 Å. Interestingly, such a large-scale expansion is partially reversible in the following cycles. Particularly, C-900 exhibits one of the best rate capability performances of 114 mAh/g at 1000 mA/g for carbon NIB anodes and stable cycling performance.

RESULTS AND DISCUSSION

In order to learn the threshold pyrolysis temperature to form soft carbon, we first conducted thermogravimetric analysis (TGA) coupled with mass spectrometry (MS) on the pyrolysis of PTCDA under argon. The selected gaseous species, including H_2O, H_2, CO_2, and CO, are monitored simultaneously. As shown in Figure S3, PTCDA loses ∼50% of the mass from 500 to 620 °C where CO and CO_2 peaks are observed in the MS plot, indicative of the removal of anhydride groups. H_2 signal is detected only at above ∼620 °C and reaches its peak relative pressure around 720 °C, suggesting the occurrence of dehydrogenation process of the aromatic carbon rings. According to the TG–MS result, we prepared a series of soft carbons by annealing PTCDA under argon at different temperatures of 700, 900, 1100, and 1600 °C. When PTCDA is heated at *T* °C, the obtained soft carbon is referred to as C-*T* (Table 1).

X-ray diffraction (XRD) patterns are collected to provide crystallinity information on the PTCDA-derived soft carbons. After pyrolysis under Ar, the long-range order of the PTCDA's crystalline structure is transformed to two broad XRD peaks of soft carbon at 2θ near 25.0° and 43.0°, indexed to (002) and (101) planes, respectively (Figure 1b). Upon increased pyrolysis temperature, the (002) peak clearly shifts to a larger angle corresponding to a smaller interlayer distance. As listed in Table 1, the interlayer distance narrows down from 3.62 Å for C-700 to 3.56 Å, 3.53 Å, and 3.46 Å for C-900, C-1100, and C-1600, respectively. We also calculated an empirical *R* value based on the ratio of the intensity at the (002) peak and the background at the equivalent peak, according to Dahn et al.'s previous study.[45] A larger *R* value indicates a higher degree of

DOI: 10.1021/acscentsci.5b00329
ACS Cent. Sci. 2015, 1, 516−522

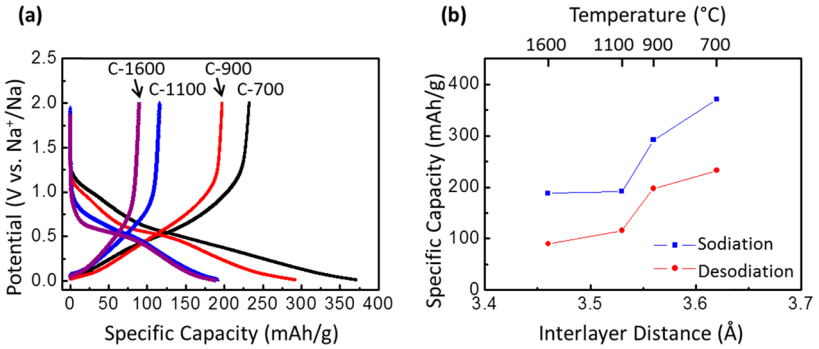

Figure 2. (a) Potential profiles for the 1st cycle of C-700, C-900, C-1100, and C-1600 tested in the potential range of 0.01−2.0 V vs Na^+/Na at 20 mA/g. (b) The first sodiation/desodiation capacity vs interlayer distance and pyrolysis temperature of soft carbons.

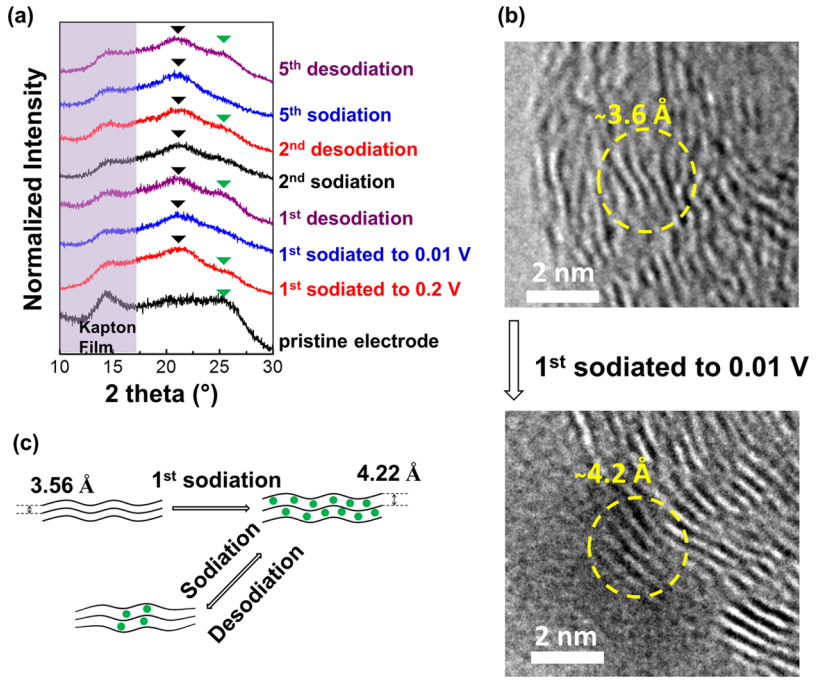

Figure 3. (a) *Ex situ* XRD patterns of C-900 electrodes during sodiation/desodiation cycling at 20 mA/g in the potential range of 0.01−2.0 V. The peaks at around 14.2° belong to the Kapton film used for *ex situ* XRD measurements. (b) *Ex situ* HRTEM images of C-900 electrodes before and after sodiation to 0.01 V at 20 mA/g. (c) Schematic representation of Na-ion storage mechanism in C-900.

graphitic order. Please see the calculation details in the Supporting Information and Figure S4. As listed in Table 1, hard carbon formed by pyrolysis of sucrose at 1100 °C exhibits an *R* value of only 1.35 while the *R* value is 1.94 for C-700 formed at 700 °C. By increasing the pyrolysis temperature, *R* values increase to 2.67 for C-900, 4.47 for C-1100, and 10.94 for C-1600, confirming the graphitizable nature of the PTCDA-derived soft carbons. The domain size along the *c*-axis of a graphitic structure can be further calculated by the Scherrer equation, where there are, on average, 3.8, 4.8, 6.2, and 13.8 layers of graphene sheets in the domains of C-700, C-900, C-1100, and C-1600 (Table 1). Please see calculation details in the Supporting Information, Figure S5, and Table S2. Overall, the XRD results suggest that both interlayer distance and graphitic domain size of the PTCDA-derived soft carbons can be adjusted by using different pyrolysis temperatures.

We further "look at" the atomistic structures of these soft carbons by transmission electron microscopy (TEM). Figure 1d,e show high-resolution TEM (HRTEM) images of C-900 and C-1100, respectively. Both samples comprise turbostratic domains that exhibit a good degree of short-range order. The diffraction rings in the selected area electron diffraction (SAED) of C-900 (Figure 1c) suggest the existence of polycrystalline graphitic structures. However, when the pyrolysis temperature rises to 1600 °C, an ordered graphitic structure appears with well-resolved lattice fringes and large graphitic crystals in C-1600 (Figure 1f). Supported by the XRD and TEM results, it is clear that the PTCDA-derived soft carbons are graphitizable and, therefore, can serve as a model of soft carbon. Moreover, scanning electron microscopy (SEM) observation provides further morphological information for PTCDA and its derived carbon products. Revealed in our previous study, PTCDA exhibits a rodlike morphology with about 1 μm length and 200 nm width (Figure S6a).[41] After pyrolysis, the resulting carbons also exhibit rodlike morphology but with much larger sizes (Figure S6). Such bulk morphologies result in a relatively low surface area.

We then studied the Na-ion storage properties of obtained soft carbons in coin cells with soft carbon-based working electrodes, sodium foil as the counter/reference electrode, and

DOI: 10.1021/acscentsci.5b00329
ACS Cent. Sci. 2015, 1, 516−522

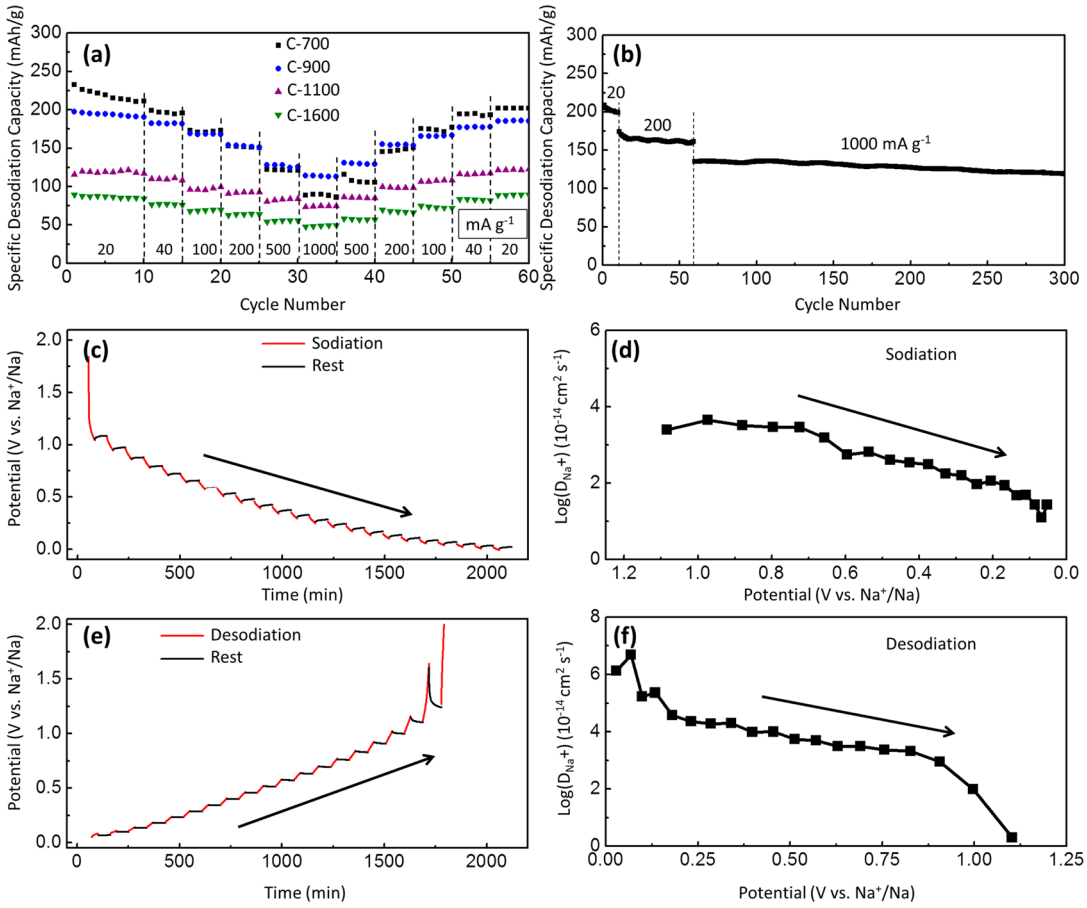

Figure 4. (a) Rate capability of soft carbons and (b) cycling performance of C-900 in the potential range of 0.01−2.0 V vs Na^+/Na. (c, e) GITT profiles of C-900 for sodiation and desodiation of the 2nd cycle, respectively. (d, f) Corresponding Na^+ diffusivity in soft carbon at different stages of charge.

an electrolyte containing 1.0 M $NaPF_6$ solution in ethylene carbon (EC)/diethyl carbonate (DEC) (1:1 in volume). The working electrodes are composed of soft carbon (80 wt %), carbon black (10 wt %), and polyvinylidene fluoride (PVdF, 10 wt %) binder. The specific capacity is calculated based on the total mass of soft carbon and carbon black. Galvanostatic sodiation/desodiation cycling at 20 mA/g is first performed in 0.01−2 V vs Na^+/Na. As Figure 2a shows, the specific capacity gradually decreases from C-700 to C-1600. C-700 exhibits the first sodiation capacity of 371 mAh/g and desodiation capacity of 233 mAh/g in contrast to 188 mAh/g and 89 mAh/g for C-1600.

All soft carbon exhibits relatively low 1st cycle CE of 62.6%, 67.6%, 60.5%, and 47.5% for C-700, C-900, C-1100, and C-1600, respectively (Table 1). The low 1st cycle CE values indicate that a large portion of Na ions are immobilized with the soft carbons, either on the surface or inside the bulk phases. If on the surface, it is attributed to the formation of solid electrolyte interphase (SEI) that is proportional to the specific surface area as we observed for hard carbon. Larger surface areas often result in lower 1st cycle CE values and low capacities.[46] However, the specific surface area of all these soft carbons is lower than 33 m^2/g, in contrast to that of a typical hard carbon, i.e., >100 m^2/g (Table 1 and Figure S7). Interestingly, the 1st cycle CE values of these soft carbons are clearly lower than those of hard carbons that exhibit higher surface areas. We then look at the hydrogen content in these soft carbons, where it is already very low for C-700 (Table 1) and thus the hydrogen residues should not be responsible for the low 1st cycle CE values. If Na ions are not trapped on surface by forming SEI, we can only hypothesize that these Na ions are irreversibly trapped inside the soft carbon graphitic galleries.

In order to bring insights to the sodiation/desodiation mechanism in soft carbons, we conducted air-free *ex situ* XRD on C-900 at different stage of charge (SOC) during sodiation/desodiation cycling. As shown in Figure 3a, after sodiation at 20 mA/g from open circuit voltage (OCV) to 0.2 V, the XRD (002) peak splits and a part of it shifts from ∼25.0° to ∼21.0° with a bump remaining at 25°. The new peak at ∼21.0° is indicative of the structure expansion of the soft carbon structure upon sodiation. With further sodiation to 0.01 V, the (002) peak completely shifts to ∼21.0°, indicating a full expansion of the interlayer spacing from 3.56 to 4.22 Å. After the first desodiation to 2.0 V, interestingly, the (002) peak splits with some peak intensity restored at ∼25.0° (Figure 3a). Importantly, as revealed in the second and fifth cycles, the attenuating and restoring of the peak intensity at ∼25.0° is highly reversible during sodiation/desodiation cycles. To our knowledge, this is the largest "breathing" scale ever known for a carbon material during electrochemical insertion/extraction of Na ions without solvent cointercalation. Note that the peak at ∼21.0° formed after the first sodiation remains in existence in the following cycles, which indicates that parts of the soft carbon structure keep expanding with Na ions trapped in the structure. This supports our hypothesis in terms of the low 1st

DOI: 10.1021/acscentsci.5b00329
ACS Cent. Sci. 2015, 1, 516−522

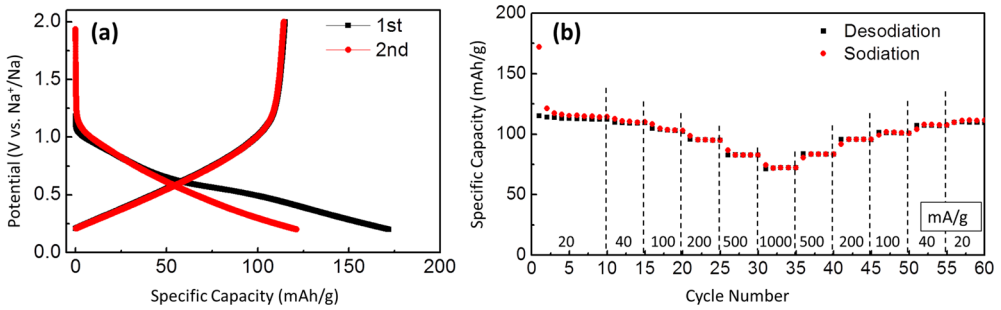

Figure 5. Galvanostatic sodiation and desodiation of C-900 tested in the potential range of 0.2−2.0 V vs Na^+/Na: (a) The first two cycles at 20 mA/g and (b) cycling performance at various current densities to test rate capability.

cycle CE. To further probe the structure transition of the soft carbon after the first sodiation, we conducted *ex situ* TEM on C-900 before and after sodiation to 0.01 V at 20 mA/g. Indeed, the interlayer distance of C-900 increases from ∼3.6 to ∼4.2 Å after the first sodiation, as shown in Figure 3b, which is well consistent with the *ex situ* XRD results. We are aware that the interlayer spacing of this electrochemically expanded soft carbon resembles that of recently reported expanded graphite (4.3 Å) reduced from graphite oxide.[47] We anticipate that such expanded structure would facilitate the fast sodiation/desodiation process and thus lead to a superior rate performance (Figure 3c). The rate and cycling performance will be discussed in later sections.

Another fundamental question is why there is a vast difference of capacities in between different soft carbons, e.g., 197 mAh/g for C-900 vs 89 mAh/g for C-1600. To explain this phenomenon, we also conducted *ex situ* XRD measurements on the C-1600 electrode upon sodiation/desodiation cycles, and found that the interlayer spacing of C-1600 is only slightly expanded upon sodiation from 3.46 to 3.52 Å (Figure S8). The small degree of expansion causes a lack of sufficient space for Na-ion storage, which explains the low capacity of C-1600. It appears that it is difficult to expand the soft carbon structures to a large degree when the interlayer distance is sufficiently small. With an interlayer distance as small as 3.56 Å in C-900, reversible insertion of Na ions takes place with a good desodiation capacity of 197 mAh/g; however, when the interlayer distance decreases to 3.53 Å for C-1100, the capacity drops over a cliff to 116 mAh/g. Such a significant capacity disparity between the two samples is remarkable, indicating that there might be a threshold value of interlayer distance below which the Na ion insertion becomes very difficult (Figure 2b).

We are also interested in the rate capability of the soft carbons evaluated at various current densities in the potential range of 0.01−2 V. As shown in Figure 4a, C-700 shows highest desodiation capacity at a current density no higher than 100 mA/g. However, when the current density is 200 mA/g or above, C-700 suffers poor capacity retention, which may be due to the poor degree of carbonization. C-900 exhibits impressive performance at higher current densities, which delivers a desodiation capacity of ∼114 mAh/g at 1000 mA/g. Please note that the capacity retention upon high current densities of C-1100 and C-1600 is good as well; however, their capacities are much lower than that of C-900. This should be attributed to their smaller interlayer distances and/or more graphitic structures. Furthermore, C-900 also delivers a stable cycling life for 300 cycles with little fading (20 mA/g for 10 cycles, 200 mA/g for 50 cycles, and then 1000 mA/g for 240 cycles, Figure 4b). Overall, C-900 shows an optimized Na-ion storage performance including relatively high capacity, acceptable 1st cycle CE, superior rate capability, and great cycling performance, which reveals a very promising NIB anode.

In order to understand the kinetics of Na ion storage in the PTCDA-derived soft carbon, measurements of the galvanostatic intermittent titration technique (GITT) are carried out. GITT on the C-900 electrode is conducted with pulse current at 20 mA/g for 30 min between rest intervals for 60 min. According to Fick's second law of diffusion, the diffusivity of sodium (D_{Na^+}) can be estimated based on the following equation:[48−50]

$$D_{Na^+} = \frac{4}{\pi\tau}\left(\frac{m_B V_M}{M_B S}\right)^2\left(\frac{\Delta E_s}{\Delta E_t}\right)^2$$

where τ is the pulse duration, m_B and M_B are the carbon active mass and molar mass of carbon, V_M is the molar volume, and S is the active surface area of the C-900 electrode. ΔE_s and ΔE_t can be obtained from the GITT curves (Figures 4c and 4e). As shown in Figure 4d, Na^+ diffusivity reaches an order of 10^{-14} cm^2/s, where it gradually decreases upon further sodiation. In the desodiation process (Figure 4f), the diffusivity drops fast at the beginning before it gradually decreases further in a higher potential range of 0.2−0.8 V. We are currently pursuing computational methods to further understand the trend of diffusivity as a function of state of charge for soft carbon.

As discussed before, different from hard carbon, soft carbons do not exhibit a flat potential plateau near 0.0 V vs Na^+/Na, which potentially enables a dendrite-free anode for NIBs if the lower cutoff potential is chosen to be moved up. To further explore this point, we increase the lower cutoff potential from 0.01 to 0.2 V vs Na^+/Na for evaluating C-900. As shown in Figure 5a, the first sodiation/desodiation capacities reach 172.0/115.1 mAh/g at 20 mA/g, giving rise to the 1st cycle CE of 66.9%, which is very similar to the case in the potential window from 0.01 to 2 V. C-900 exhibits an excellent rate performance in this potential window as well, which delivers a desodiation capacity of 72 mAh/g at a high current density of 1000 mA/g (Figure 5b). Also importantly, in this voltage window, C-900 shows a stable cycling performance as well (Figure S9).

To further explore using 0.2 V as the cutoff potential for soft carbon, we conduct cyclic voltammetry (CV) measurements on C-900 and compare the result with a typical hard carbon. It is evident that a major cathodic sodiation reaction occurs on soft carbon above 0.2 V while sodiation of hard carbon mainly happens below 0.2 V (Figure S10).[30,31,51] We also measure the CV of C-900 in the potential window of 0.2−2.0 V, where reversible sodiation/desodiation reactions are also observed. To further demonstrate that 0.2 V is far above from the plating

DOI: 10.1021/acscentsci.5b00329
ACS Cent. Sci. 2015, 1, 516−522

potential, we conduct deep sodiation, where Na starts to plate on soft carbon surface at −0.035 V vs Na^+/Na (Figure S11). A further point we raise is that soft carbon exhibits a large portion of its capacity above 0.2 V, which is a clear advantage over hard carbons because the latter has more than 50% of its capacity from the plateau region near 0 V.

CONCLUSION

In summary, this work demonstrates that soft carbon can be competitive to hard carbon if a suitable precursor is chosen and treated at selected conditions. Previously, only hard carbon had been known for its good capacities in NIBs. To identify alternative carbons as NIB anodes is of great fundamental and practical values for the field of NIBs. Furthermore, we discover that there is a subtle correlation between the capacities of soft carbons and the interlayer spacing, where a narrower interlayer spacing is found linked to a lower capacity. For the first time, we identify that the interlayer distance of soft carbon is electrochemically expandable, i.e., from 3.6 Å to ∼4.2 Å after the first sodiation. As revealed by *ex situ* XRD patterns, parts of this expansion are irreversible, which rationalizes the low 1st cycle coulombic efficiency. On the other hand, parts of the expansion are reversible, which explains the high capacity and excellent cycling performance. Among different samples, C-900 with an interlayer distance of 3.56 Å exhibits an optimal overall performance with a high reversible capacity, superior rate capability, and stable cycling performance. Moreover, C-900 can be a safer carbon anode for NIBs, which delivers great performance in the potential range of 0.2−2.0 V as well. Our results provide insights on future studies of soft carbon as potential high-rate anode materials in NIBs.

ASSOCIATED CONTENT

Supporting Information

The Supporting Information is available free of charge on the ACS Publications website at DOI: 10.1021/acscentsci.5b00329.

Experimental section, characterization details, and supporting data (PDF)

AUTHOR INFORMATION

Corresponding Author

*E-mail: david.ji@oregonstate.edu.

Author Contributions

†W.L. and Z.J. contributed equally to this work.

Notes

The authors declare no competing financial interest.

ACKNOWLEDGMENTS

We acknowledge the financial support from Advanced Research Projects Agency-Energy (ARPA-E), Department of Energy of the United States, Award No. DE-AR0000297TDD. We appreciate the help from Joshua Razink for his kind help in TEM measurements in CAMCOR. We are grateful to Professor Douglas A. Keszler for ex situ XRD measurements. The authors appreciate Dr. Jong-Jan Lee, Dr. Sean Vail, and Dr. Yuhao Lu from Sharp Laboratories America for their assistance and advice.

REFERENCES

(1) Yang, Z.; Zhang, J.; Kintner-Meyer, M. C. W.; Lu, X.; Choi, D.; Lemmon, J. P.; Liu, J. Electrochemical energy storage for green grid. *Chem. Rev.* **2011**, *111*, 3577−3613.

(2) Yang, Y.; Zheng, G.; Cui, Y. Nanostructured sulfur cathodes. *Chem. Soc. Rev.* **2013**, *42*, 3018−3032.

(3) Lu, J.; Li, L.; Park, J.-B.; Sun, Y.-K.; Wu, F.; Amine, K. Aprotic and aqueous $Li-O_2$ batteries. *Chem. Rev.* **2014**, *114*, 5611−5640.

(4) Mai, L.; Tian, X.; Xu, X.; Chang, L.; Xu, L. Nanowire electrodes for electrochemical energy storage devices. *Chem. Rev.* **2014**, *114*, 11828−11862.

(5) Whittingham, M. S. Ultimate limits to intercalation reactions for lithium batteries. *Chem. Rev.* **2014**, *114*, 11414−11443.

(6) Xu, K. Electrolytes and interphases in Li-ion batteries and beyond. *Chem. Rev.* **2014**, *114*, 11503−11618.

(7) Tarascon, J. M.; Armand, M. Issues and challenges facing rechargeable lithium batteries. *Nature* **2001**, *414*, 359−367.

(8) Choi, N.-S.; Chen, Z.; Freunberger, S. A.; Ji, X.; Sun, Y.-K.; Amine, K.; Yushin, G.; Nazar, L. F.; Cho, J.; Bruce, P. G. Challenges facing lithium batteries and electrical double-layer capacitors. *Angew. Chem., Int. Ed.* **2012**, *51*, 9994−10024.

(9) Kim, S.-W.; Seo, D.-H.; Ma, X.; Ceder, G.; Kang, K. Electrode materials for rechargeable sodium-ion batteries: potential alternatives to current lithium-ion batteries. *Adv. Energy Mater.* **2012**, *2*, 710−721.

(10) Slater, M. D.; Kim, D.; Lee, E.; Johnson, C. S. Sodium-ion batteries. *Adv. Funct. Mater.* **2013**, *23*, 947−958.

(11) Pan, H.; Hu, Y.-S.; Chen, L. Room-temperature stationary sodium-ion batteries for large-scale electric energy storage. *Energy Environ. Sci.* **2013**, *6*, 2338−2360.

(12) Yabuuchi, N.; Kubota, K.; Dahbi, M.; Komaba, S. Research development on sodium-ion batteries. *Chem. Rev.* **2014**, *114*, 11636−11682.

(13) Lee, H.-W.; Wang, R. Y.; Pasta, M.; Woo Lee, S.; Liu, N.; Cui, Y. Manganese hexacyanomanganate open framework as a high-capacity positive electrode material for sodium-ion batteries. *Nat. Commun.* **2014**, *5*, 5280.

(14) Li, S.; Dong, Y.; Xu, L.; Xu, X.; He, L.; Mai, L. Effect of carbon matrix dimensions on the electrochemical properties of $Na_3V_2(PO_4)_3$ nanograins for high-performance symmetric sodium-ion batteries. *Adv. Mater.* **2014**, *26*, 3545−3553.

(15) Chen, C.; Wen, Y.; Hu, X.; Ji, X.; Yan, M.; Mai, L.; Hu, P.; Shan, B.; Huang, Y. Na^+ intercalation pseudocapacitance in graphene-coupled titanium oxide enabling ultra-fast sodium storage and long-term cycling. *Nat. Commun.* **2015**, *6*, 6929.

(16) Oh, S.-M.; Myung, S.-T.; Yoon, C. S.; Lu, J.; Hassoun, J.; Scrosati, B.; Amine, K.; Sun, Y.-K. Advanced $Na[Ni_{0.25}Fe_{0.5}Mn_{0.25}]O_2/C-Fe_3O_4$ Sodium-ion batteries using EMS electrolyte for energy storage. *Nano Lett.* **2014**, *14*, 1620−1626.

(17) Ellis, B. L.; Nazar, L. F. Sodium and sodium-ion energy storage batteries. *Curr. Opin. Solid State Mater. Sci.* **2012**, *16*, 168−177.

(18) Kundu, D.; Talaie, E.; Duffort, V.; Nazar, L. F. The emerging chemistry of sodium ion batteries for electrochemical energy storage. *Angew. Chem., Int. Ed.* **2015**, *54*, 3431−3448.

(19) Palomares, V.; Serras, P.; Villaluenga, I.; Hueso, K. B.; Carretero-Gonzalez, J.; Rojo, T. Na-ion batteries, recent advances and present challenges to become low cost energy storage systems. *Energy Environ. Sci.* **2012**, *5*, 5884−5901.

(20) Kim, Y.; Ha, K.-H.; Oh, S. M.; Lee, K. T. High-capacity anode materials for sodium-ion batteries. *Chem. - Eur. J.* **2014**, *20* (38), 11980−11992.

(21) Dahbi, M.; Yabuuchi, N.; Kubota, K.; Tokiwa, K.; Komaba, S. Negative electrodes for Na-ion batteries. *Phys. Chem. Chem. Phys.* **2014**, *16*, 15007−15028.

(22) Bommier, C.; Ji, X. Recent development on anodes for Na-ion batteries. *Isr. J. Chem.* **2015**, *55*, 486−507.

(23) Sun, J.; Lee, H.-W.; Pasta, M.; Yuan, H.; Zheng, G.; Sun, Y.; Li, Y.; Cui, Y. A phosphorene−graphene hybrid material as a high-capacity anode for sodium-ion batteries. *Nat. Nanotechnol.* **2015**, *10*, 980−985.

(24) Kim, K.-T.; Ali, G.; Chung, K. Y.; Yoon, C. S.; Yashiro, H.; Sun, Y.-K.; Lu, J.; Amine, K.; Myung, S.-T. Anatase titania nanorods as an intercalation anode material for rechargeable sodium batteries. *Nano Lett.* **2014**, *14*, 416−422.

DOI: 10.1021/acscentsci.5b00329
ACS Cent. Sci. 2015, 1, 516−522

(25) Fan, X.; Mao, J.; Zhu, Y.; Luo, C.; Suo, L.; Gao, T.; Han, F.; Liou, S.-C.; Wang, C. Superior Stable Self-Healing SnP_3 Anode for Sodium-Ion Batteries. *Adv. Energy Mater.* **2015**, *5*, 1500174.
(26) Zhu, Y.; Wen, Y.; Fan, X.; Gao, T.; Han, F.; Luo, C.; Liou, S.-C.; Wang, C. Red Phosphorus−Single-Walled Carbon Nanotube Composite as a Superior Anode for Sodium Ion Batteries. *ACS Nano* **2015**, *9*, 3254−3264.
(27) Ge, P.; Fouletier, M. Electrochemical intercalation of sodium in graphite. *Solid State Ionics* **1988**, *28-30*, 1172−1175.
(28) Jache, B.; Adelhelm, P. Use of graphite as a highly reversible electrode with superior cycle life for sodium-ion batteries by making use of co-intercalation phenomena. *Angew. Chem., Int. Ed.* **2014**, *53*, 10169−10173.
(29) Cao, Y.; Xiao, L.; Sushko, M. L.; Wang, W.; Schwenzer, B.; Xiao, J.; Nie, Z.; Saraf, L. V.; Yang, Z.; Liu, J. Sodium ion insertion in hollow carbon nanowires for battery applications. *Nano Lett.* **2012**, *12*, 3783−3787.
(30) Stevens, D. A.; Dahn, J. R. High capacity anode materials for rechargeable sodium-ion batteries. *J. Electrochem. Soc.* **2000**, *147*, 1271−1273.
(31) Stevens, D. A.; Dahn, J. R. The mechanisms of lithium and sodium insertion in carbon materials. *J. Electrochem. Soc.* **2001**, *148*, A803−A811.
(32) Tang, K.; Fu, L.; White, R. J.; Yu, L.; Titirici, M.-M.; Antonietti, M.; Maier, J. Hollow carbon nanospheres with superior rate capability for sodium-based batteries. *Adv. Energy Mater.* **2012**, *2*, 873−877.
(33) Komaba, S.; Murata, W.; Ishikawa, T.; Yabuuchi, N.; Ozeki, T.; Nakayama, T.; Ogata, A.; Gotoh, K.; Fujiwara, K. Electrochemical Na insertion and solid electrolyte interphase for hard-carbon electrodes and application to Na-Ion batteries. *Adv. Funct. Mater.* **2011**, *21*, 3859−3867.
(34) Luo, W.; Bommier, C.; Jian, Z.; Li, X.; Carter, R.; Vail, S.; Lu, Y.; Lee, J.-J.; Ji, X. Low-surface-area hard carbon anode for Na-ion batteries via graphene oxide as a dehydration agent. *ACS Appl. Mater. Interfaces* **2015**, *7*, 2626−2631.
(35) Dahn, J. R.; Zheng, T.; Liu, Y.; Xue, J. S. Mechanisms for lithium insertion in carbonaceous materials. *Science* **1995**, *270*, 590−593.
(36) Doeff, M. M.; Ma, Y.; Visco, S. J.; De Jonghe, L. C. Electrochemical insertion of sodium into carbon. *J. Electrochem. Soc.* **1993**, *140*, L169−L170.
(37) Alcántara, R.; Jiménez-Mateos, J. M.; Lavela, P.; Tirado, J. L. Carbon black: a promising electrode material for sodium-ion batteries. *Electrochem. Commun.* **2001**, *3*, 639−642.
(38) Pol, V. G.; Lee, E.; Zhou, D.; Dogan, F.; Calderon-Moreno, J. M.; Johnson, C. S. Spherical carbon as a new high-rate anode for sodium-ion batteries. *Electrochim. Acta* **2014**, *127*, 61−67.
(39) Qie, L.; Chen, W.; Xiong, X.; Hu, C.; Zou, F.; Hu, P.; Huang, Y. Sulfur-doped carbon with enlarged interlayer distance as a high-performance anode material for sodium-ion batteries. *Adv. Sci.* **2015**, DOI: 10.1002/advs.201500195.
(40) Li, W.; Zhou, M.; Li, H.; Wang, K.; Cheng, S.; Jiang, K. A high performance sulfur-doped disordered carbon anode for sodium ion batteries. *Energy Environ. Sci.* **2015**, *8*, 2916−2921.
(41) Luo, W.; Allen, M.; Raju, V.; Ji, X. An organic pigment as a high-performance cathode for sodium-ion batteries. *Adv. Energy Mater.* **2014**, *4*, 1400554.
(42) Han, X.; Chang, C.; Yuan, L.; Sun, T.; Sun, J. Aromatic carbonyl derivative polymers as high-performance Li-ion storage materials. *Adv. Mater.* **2007**, *19*, 1616−1621.
(43) Wang, H. g.; Yuan, S.; Ma, D. l.; Huang, X. l.; Meng, F. l.; Zhang, X. b. Tailored aromatic carbonyl derivative polyimides for high-power and long-cycle sodium-organic batteries. *Adv. Energy Mater.* **2014**, *4*, 1301651.
(44) Hara, M.; Satoh, A.; Takami, N.; Ohsaki, T. Structural and electrochemical properties of lithiated polymerized aromatics. Anodes for lithium-ion cells. *J. Phys. Chem.* **1995**, *99*, 16338−16343.
(45) Liu, Y.; Xue, J. S.; Zheng, T.; Dahn, J. R. Mechanism of lithium insertion in hard carbons prepared by pyrolysis of epoxy resins. *Carbon* **1996**, *34*, 193−200.
(46) Bommier, C.; Luo, W.; Gao, W.-Y.; Greaney, A.; Ma, S.; Ji, X. Predicting capacity of hard carbon anodes in sodium-ion batteries using porosity measurements. *Carbon* **2014**, *76*, 165−174.
(47) Wen, Y.; He, K.; Zhu, Y.; Han, F.; Xu, Y.; Matsuda, I.; Ishii, Y.; Cumings, J.; Wang, C. Expanded graphite as superior anode for sodium-ion batteries. *Nat. Commun.* **2014**, *5*, 4033.
(48) Weppner, W.; Huggins, R. A. Determination of the kinetic parameters of mixed-conducting electrodes and application to the system Li_3Sb. *J. Electrochem. Soc.* **1977**, *124*, 1569−1578.
(49) Shaju, K. M.; Subba Rao, G. V.; Chowdari, B. V. R. Electrochemical kinetic studies of Li-ion in O_2-structured $Li_{2/3}(Ni_{1/3}Mn_{2/3})O_2$ and $Li_{(2/3)+x}(Ni_{1/3}Mn_{2/3})O_2$ by EIS and GITT. *J. Electrochem. Soc.* **2003**, *150*, A1−A13.
(50) Zhu, Y.; Wang, C. Galvanostatic intermittent titration technique for phase-transformation electrodes. *J. Phys. Chem. C* **2010**, *114*, 2830−2841.
(51) Luo, W.; Schardt, J.; Bommier, C.; Wang, B.; Razink, J.; Simonsen, J.; Ji, X. Carbon nanofibers derived from cellulose nanofibers as a long-life anode material for rechargeable sodium-ion batteries. *J. Mater. Chem. A* **2013**, *1*, 10662−10666.

DOI: 10.1021/acscentsci.5b00329
ACS Cent. Sci. 2015, 1, 516−522